Validation of Astrodynamic Formation Flying Models Against SPACE-SI Experiments with Prisma Satellites

Drago Matko, Tomaž Rodič, Sašo Blažič, Aleš Marsetič, Krištof Oštir, Gašper Mušič, Luka Teslić, Gregor Klančar, Marko Peljhan, David Zobavnik
Space-SI
Aškerčeva cesta 12, 1000 Ljubljana, Slovenia; +386-1-4768-252
drago.matko@space.si, tomaz.rodic@space.si, saso.blazic tomaz.rodic@space.si,kristof.ostir@space.si, gasper.music@space.si, luka.teslic@space.si, gregor.klancar@space.si, marko.peljhan@space.si, david.zobavnik@gmail.com

Robin Larsson, Eric Clacey, Christian Svärd, Thomas Karlsson
OHB Sweden AB,
SE-171 22 Solna, Sweden; +46 (0) 8 627 64 40
robin.larsson@ohb-sweden.se eric.clacey@ohb-sweden.se, christian.sward@ohb-sweden.se, thomas.karlsson@ohb-sweden.se

ABSTRACT

In this paper several astrodynamical formation flying models are assessed against the experimental results derived from the SPACE-SI formation flying experiments performed in September 2011with the OHB Sweden developed Prisma satellites Mango and Tango. In these formation flying experiments critical manoeuvres for three types of missions were investigated with respect to in-orbit performances. The experiments included parallel flying with in-track displacement demonstrating high-resolution optical dual satellite imaging and radar interferometric constellation, circumvolution as well as encircling of the target demonstrating debris observation and parallel flying with the radial displacement demonstrating fractionated spacecraft and accurate pointing of the formation. The astrodynamic data of the experiment are used to verify several formation flying models including a nonlinear model, a linear Hill-Clohessy-Wiltshire model, STK models with four propagators (Earth mass point, J2, default HPOP and HPOP with all disturbances) and the hereby originally proposed extension to the Hill-Clohessy-Wiltshire model, a linear model for orbits with small eccentricities.

INTRODUCTION

In this paper seven astrodynamics formation flying models are assessed against the experimental results derived from the SPACE-SI formation flying experiments that were performed with the Prisma [1, 2, 3, 4] satellites Mango and Tango developed by OHB Sweden. The motivation for this study steams from the needs for reliable data and models that will be required to analyse various formation flying concepts including distributed instruments geometries for astronomy, communications, metrology and remote sensing of Earth as well as in-orbit inspections and servicing. To investigate these scenarios SPACE-SI and OHB Sweden performed a set of formation flying experiments in September 2011 with the Prisma satellites Mango and Tango, that were launched into a sun synchronous orbit with 725 km altitude and 06.00h ascending node in June 2010. In the SPACE-SI formation flying experiments critical maneuvers for three types of missions were investigated with respect to the in-orbit performances.

In the Prisma mission Mango and Tango are flying close to each other, therefore close formation flying will be discussed in the paper, i.e. the satellites will be considered to fly at distances ranging from five to few hundred meters. In spacecraft formation flying mission design the relative spacecraft position is more important than the knowledge of the absolute position of the formation. In addition, knowledge of the relative states of spacecraft in a formation is often far more accurate than knowledge of the formation's absolute state. For these reasons, the theoretical part of this paper will be focused on studies of the relative positions of two spacecraft which are forming a close formation. We will use the common terms leader and follower to describe them. The leader is supposed to be in the centre of the local vertical/local horizontal (LVLH), sometimes also called Radial/In-track/Cross-track (RIC), coordinate system [5,6]. Its coordinates will be always at the origin and its absolute position (orbit) will not be controlled. The leader may also be called target satellite since in some manoeuvres it will represent the

target to be observed or approached. In the Prisma mission Mango is the main satellite and Tango the target. In our case Mango represents the follower while Tango represents the leader. This is due to the fact that Mango is chasing Tango.

The paper is organized as follows: First the SPACE-SI experiments on Prisma satellites are briefly described. Afterwards the well-known formation models are shortly outlined. An extension of the Hill-Clohessy-Wiltshire (HCW) model to orbits with small eccentricity is derived by the method of small perturbation, which is the main contribution of this paper. Further, an analytical solution of the linear model for small eccentricity is given and the paper concludes with the validation of the models against the Prisma experiment.

FORMATION FLYING EXPERIMENTS

In September 2011, on the Prisma satellites Mango and Tango that were launched into a sun synchronous orbit with 725 km altitude and 06.00h ascending node in June 2010, SPACE-SI and OHB Sweden performed a series of experiments involving critical maneuvers for three mission types with respect to in-orbit performance, to investigate formation flying paradigms.

In-Flight Simulated Radar Interferometry

Formation flying capabilities are especially important for satellite based radar interferometry (InSAR), one of the more interesting applications for the acquisition of synthetic aperture radar imagery. Because the phase angle of the backscattered signal for a given pixel is available, and phase is easily measured, it is possible to compare the phase differences of two different images of the same region and, from that comparison the relative locations of pixels in three dimensions is found [7]. The interferometry is using radar images, acquired from slightly different positions which correspond to different orbits. By comparing the phase (Φ, and the phase difference $\Delta\Phi$) of a pair of images the height of the reflection and the shape of the surface (digital elevation model, DEM) can be determined. Depending on the imaging configuration, surface changes (i.e. displacements, movements) can also be observed.

One can obtain the best results with a satellite constellation, where a pair of satellites is in two different orbits that are separated by a distance of several hundred meters (e.g. 100-200 m). The satellites can be either in the same orbit (along-track) or in parallel orbits (across-track). One of the satellites emits a radar signal, while both of them receive the signal. During imaging the relative separation of the satellites has to be stable and precisely known (in the range of millimeters) to enable interferometric processing and achieve optimal results [7].

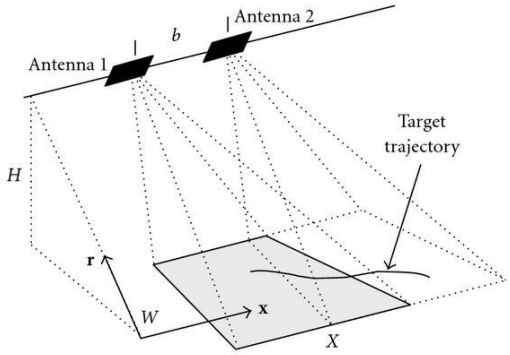

Fig 1. Along-track interferometric geometry

With the Prisma experiment we have tested the along-track interferometric configuration (see Fig. 1). Along-track synthetic aperture radar interferometry is currently not widely in use since the only system capable of providing it is the German TanDEM-X constellation, developed by DLR, EADS Astrium and Infoterra [7,8]. It offers, however, entirely new opportunities. This application uses two separate radar antennas arranged longitudinally along the direction of flight; a method that permits the measurement of the speed of moving objects, as the two satellites image the same area successively, with a brief interval in between. The method is used particularly in oceanography, glaciology, and traffic research [9]. For successful determination of speed measurements an optimal distance between the satellites (so called baseline) has to be used and maintained. It has been proven that the baseline should be between hundred and several hundred meters [7].

In our experiment the Tango and Mango satellites were positioned at a distance of approximately 200 m along-track and the relative position was maintained for three consecutive orbits. Natural forces have influenced the relative position of the satellites. We have observed the stability of the formation and have allowed small drifting of the satellites, since these can be detected and corrected in InSAR processing. We have observed the absolute and relative position of both satellites. The Prisma constellation has proven to have the stability that is required for interferometric data processing [10]. All the drifting effects are small and can be removed in the processing step. The orbital stability and accuracy influence the estimated accuracy of velocity measurements obtained with along track interferometry. We have estimated that the water current speeds accuracy of 0.05 m/s can be obtained. In a similar across-track constellation with similar orbital

parameters and orbital accuracy the vertical accuracy of the digital elevation model production could reach 1 m.

The astrodynamic data of this experiment are used to verify the formation flying models in Section Validation of the Models Against Prisma Experiment.

Observation of Non Cooperative Objects–space debris

It is expected that non-cooperative objects such as space debris will become a serious problem in the near future. Debris orbits often overlap with trajectories of operational spacecraft, and represent a potential collision risk. In order to remove or mitigate the debris collision risk, it must be first identified. To simulate the required procedures, two experiments were performed: orbit identification and close observation.

On the basis of the space debris Two Line Elements (TLE) the Mango's camera was directed in the direction of the point of the closest approach and several images were taken in a sequence. The Simulation toolkit (AGI - STK) was used to simulate the trajectories of Mango and the debris. The newest TLE database was used to identify the satellites or debris flying closer than 25km to Mango as well as the corresponding time frame. The criteria for choosing the objet to be observed with Mango vision based camera (VBS), was the distance and the vicinity period. Besides these two criteria additional constraints were also considered. During imaging the camera should not be pointing neither towards the Sun (the azimuth of the camera targeting the object was limited to the range between 180° and 360° according to the VVLH coordinate system) nor towards the Earth (the elevation was limited to the values larger than -20° according to the VVLH coordinate system).

In the simulations, the Geosat satellite (ID number 15595) was chosen for observation. The optimal time of closest approach was September 20, 2011 09:26:54.000. The Mango VBS was pointed in the calculated direction and several images were taken in a sequence. Three consecutive shots, taken by the VBS camera, were compared with the STK simulations to prove the viability of the procedure. The Geosat can be clearly seen in the second shot shown in Fig. 2.

Just one minute before the Geosat closest approach, the satellite SL-14 R/B with ID number 22237 was also recorded by the VBS camera in two consecutive shots, shown in Figs 3 and 4 respectively. The experiment has shown, that it is possible to predict close encounters between two satellites (including debris), as documented in details in [12].

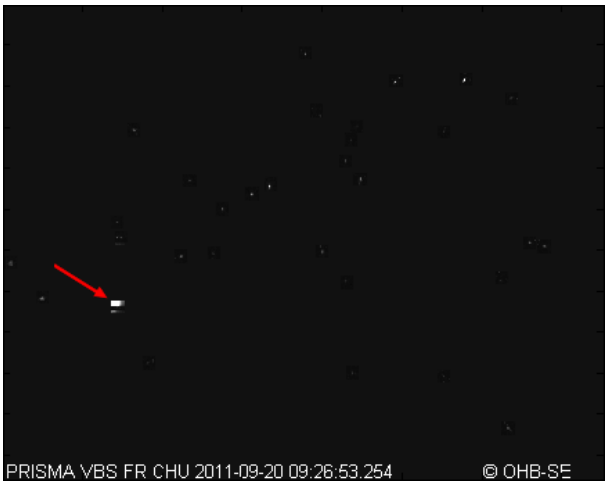

Fig. 2: VBS camera shot at 2011 09 20, 09:26:53.254

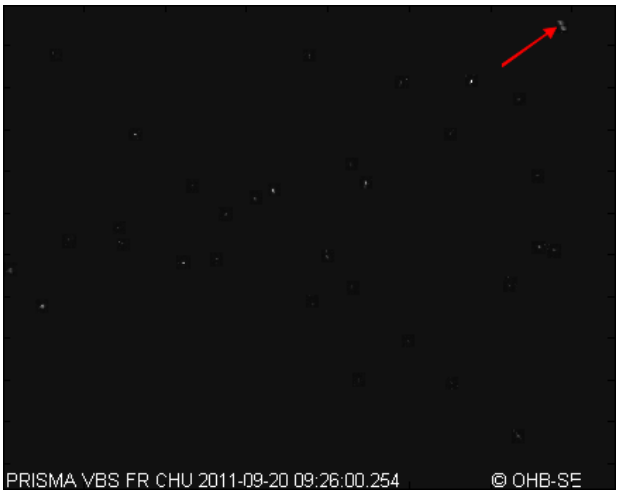

Fig. 3: VBS camera shot at 2011 09 20, 09:26:00.254

Close observation was also performed with the satellites flown in the (in-track) distance of 5 m. Mango was pointing with its Digital Video System (DVS) camera all times towards Tango, which was rotating around (with a bit of wobbling) its cross-track axis, pointing all times with its solar panels toward the sun. Several pictures of Tango (which simulated the debris) were taken in order to make a 3D model of the observed object. From the captured figures the 3D model reconstruction was performed. The reconstruction was satisfactory with the views provided by the DVS camera, while the reconstruction of the parts that were not imaged (or marginally – due to wobbling) was degraded. A better 3D model would be obtained with the use of an accurately calibrated camera on the imaging spacecraft. In order to have diversified images, also an encircling of Tango by Mango in a relative 60 degrees inclined orbit on a circle with radius 20 m was performed. Corresponding images (with far less detail)

are still being processed. The timing of imaging (during encircling) was adjusted to have some areas of interest on the Earth (Kuwait, shown in Fig 5, Djibouti, Crete) in the background.

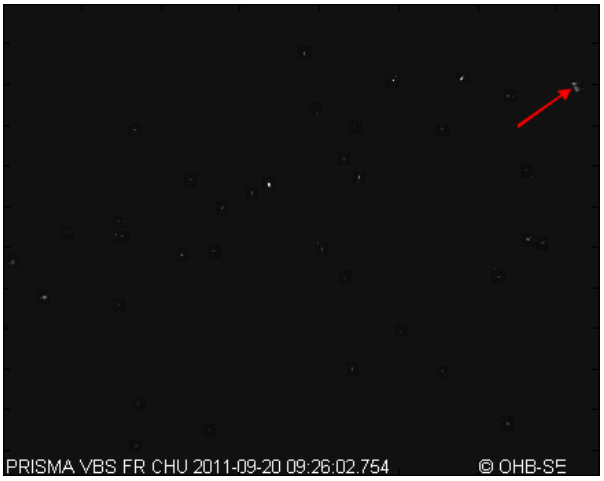

Fig. 4: VBS camera shot at 2011 09 20, 09:26:02.754

In Flight Simulated Distributed Instrument

Precise formation flying of small satellites can also lead to interesting scenarios for optical remote sensing. One of these is when a satellite camera is formed by two satellites flying one above the other or one after the other. To obtain high multispectral resolution and to keep the combined instrument as small as possible both satellites should be placed close to each other, in the range of less than 5 m. One of the satellites holds the optical system with lenses and/or mirrors and the other one the detectors (sensors).

In this case the idea is to form a telescope that can acquire high-resolution multispectral images of the Earth's surface with the use of two small satellites instead of one big and more expensive satellite. If the satellites fly one after the other (along-track) then one of the satellites must carry a mirror at an angle of approximately 45° that reflects the beam to the detectors on the other satellite. This formation is preferable as the consumption of propellant is very small. Regarding the imaging types, there are two possibilities for acquiring images. If a linear scanner is used a sweeping motion can be exploited that can cover a larger area. The other type is the "pointing mode" acquisition that can also be used when the same area is imaged during various times. In this case a full frame detector that covers a smaller area would be needed. In this experiment the Tango was simulating the holder of the optical system with lenses and/or mirrors while Mango, simulating the holder of detectors (sensors), was driven to an appropriate position. This experiment was performed in two different versions: in-track and cross-track.

Fig. 5: The DVS shot of the Persian Gulf with Tango in the foreground.

With the in-track displacement a very precise formation flying geometry is needed. To avoid blurred images when imaging, both systems have to be precisely aligned and kept at a constant relative distance and orientation. The satellites were flown in approximately the same orbit (parallel flying – in-track displacement). Inn this constellation a mirror would have to be placed at an angle of approximately 45° to reflect the beam to the sensors.

We have tested the above mentioned configuration where Mango and Tango were positioned one after the other at a relative distance of approximately 5 m. The position was kept for two orbits. During these orbits the absolute and relative position and attitude of the satellites were measured. From the obtained data we assessed the stability and capability of the formed instrument for high-resolution imaging. The results showed quite an instable motion of the satellites during both orbits. Figure 6 shows the degree of change in the viewing direction of Mango body axis. The changes are mainly below 0.1 degrees in all axes but contain major fluctuations that can reach values over 1 degree due to orbit thrusting. This means at least approximately a 1 cm pointing shift. The situation with Tango is even worse as the axis deviate more than 20 degrees due to Tango having only a 3-axis magnetic body control [13].

The relative position of the satellites was maintained with the use of Mango thrusters that regulated the

satellite motion. During the orbits the relative distance between the satellites changed up to more than 10 cm in all axes (Fig 7). The variations are relatively small but show clear instability. The flight direction axis showed the highest stability.

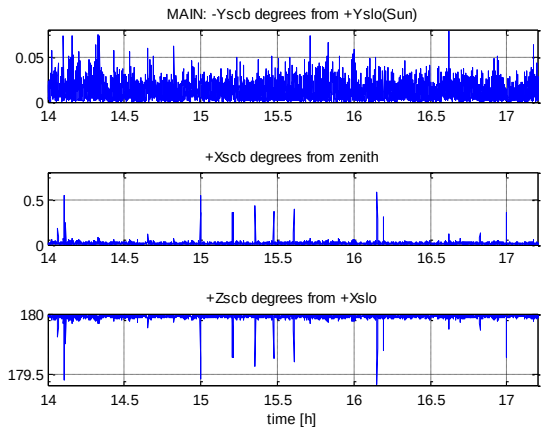

Figure 6: Changes of attitude for all Mango axes during the two consecutive orbits.

From the obtained results we can conclude that the regulation accuracy of the relative distance and attitudes are inadequate for a distributed instrument where relative positions and attitude shifts of satellites involved should be kept within millimeters. This is true both for line scanner and for a full frame camera because of the axis instability that also cannot be predicted accurately.

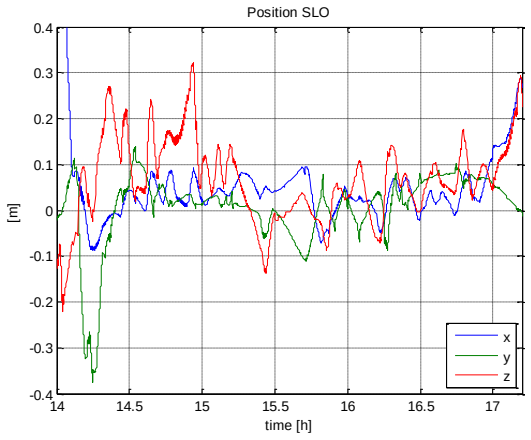

Figure 7: Relative distance variations between the satellites during two consecutive orbits (5 m have been subtracted from the – requested – along-track distance).

For satisfactory results both satellites should include reaction wheels, thrusters with a precise regulation as well as a precise relative navigation system. Relative GPS navigation as used in this experiment is not a suitable choice when position accuracy of millimeter accuracy is targeted.

With the radial and cross-track displacement the satellites were flown in slightly different orbits (parallel flying – radial and cross-track displacement). The satellites were aligned with predefined target locations on the Earth, including Cape Town (South Africa), Piran (Slovenia) and Punta Arenas (Chile). The experiment was initially planned for July, however, due to delays it was shifted to mid-September – the time of autumnal equinox. This is an inappropriate time for imaging the Earth's surface from a dusk-dawn orbit. In addition due to the inclination of the orbit the targets on the southern hemisphere had much better lighting condition than those on the northern, where our preferred area of interest Piran/Portorož, the venue of the 2012 Small Satellites Systems and Services (4S) Symposium, was located.

Orbitron [14] was used to determine the approximate time of an appropriate passage. The approximate time and the TLE data of Tango were supplied to a Matlab [15] based satellite simulator, which calculated the closest satellite position with respect to the target. Using the satellite-target vector and desired Mango-Tango distance the relative position of Mango in the Tango co-ordinate system was calculated and supplied to the STK [16] program for verification. The orientation of Tango was unchanged (the solar panels facing the Sun), while Mango was turned to track the ground target with its DVS camera during the passage. While performing this experiment on September 21, lighting conditions and weather played an important role, as described in details in [12]. Fig. 8 depicts the STK verification and the outcome of the In Flight Simulated Distributed Instrument Remote Sensing experiment for the Cape Town target, where the 62nd International Astronautical Congress was held one month later.

FORMATION FLYING MODELS

In this Section different models, which will be studied in later Sections, are presented. With respect to the experiment with the Prisma formation, the local co-ordinate system will be fixed to the target (Tango) satellite, which has no orbit control, while the orbit controlled satellite (Mango) will be named main.

Nonlinear model

Formation flying can be described by the following set of nonlinear equations [5,6]

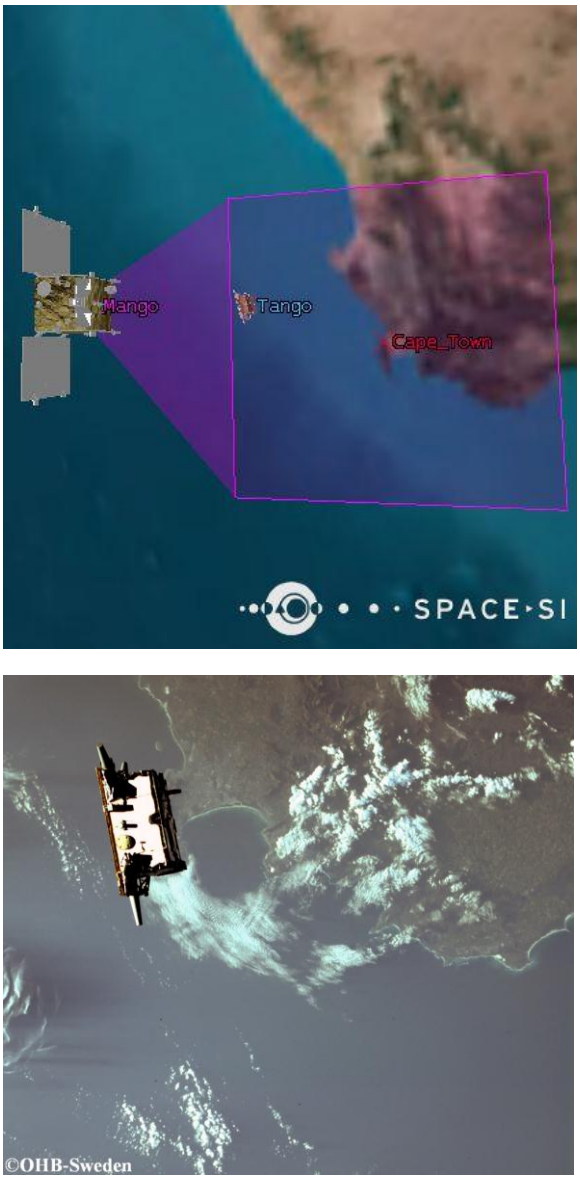

Fig. 8: The STK simulated (upper) and real DVS (lower) shot of Cape Town.

$$\begin{aligned}
\ddot{x}_n - 2\dot{\varphi}_R\dot{y}_n - \ddot{\varphi}_R y_n - \dot{\varphi}_R^2 x_n &= -\frac{\mu(R+x_n)}{((R+x_n)^2 + y_n{}^2 + z_n{}^2)^{\frac{3}{2}}} + \frac{\mu}{R^2} + a_x \\
\ddot{y}_n + 2\dot{\varphi}_R\dot{x}_n + \ddot{\varphi}_R x_n - \dot{\varphi}_R^2 y_n &= -\frac{\mu y_n}{((R+x_n)^2 + y_n{}^2 + z_n{}^2)^{\frac{3}{2}}} + a_y \\
\ddot{z}_n &= -\frac{\mu z_n}{((R+x_n)^2 + y_n{}^2 + z_n{}^2)^{\frac{3}{2}}} + a_z
\end{aligned} \tag{1}$$

where x_n (Radial), y_n (In-track) and z_n (Cross-track) are the coordinates of the main satellite in the target satellite coordinate system (called Radial/In-track/Cross-track − RIC) and a_x, a_y, a_z are the accelerations of the main satellite in the radial, in-track and cross-track direction, respectively. In the above equations R is the distance of the target satellite from Earth mass point, μ the Earth gravitational constant, and φ_R the true anomaly of the target.

The movement of the target satellite is described by the following nonlinear equations:

$$\ddot{R} = R\dot{\varphi}_R^2 - \frac{\mu}{R^2} \tag{2}$$

$$\ddot{\varphi}_R = -\frac{2\dot{R}\dot{\varphi}_R}{R}. \tag{3}$$

These equations include the influence of the eccentricity and nonlinear differential gravitation, however do not include disturbances, such as oblateness of the earth (e.g. J2 coefficient) and third bodies influences. The model is realized within STK as Earth mass point propagator.

Hill-Clohessy-Wiltshire (HCW) model

For close formation flying and small eccentricities Equations () can be linearized [6], yielding a set of linear equations with time-varying parameters

$$\begin{aligned}
\ddot{x}_L - 2\dot{\varphi}_R\dot{y}_L - \ddot{\varphi}_R y_L - \dot{\varphi}_R^2 x_L &= \frac{2\mu}{R^3}x_L + a_x \\
\ddot{y}_L + 2\dot{\varphi}_R\dot{x}_L + \ddot{\varphi}_R x_L - \dot{\varphi}_R^2 y_L &= -\frac{\mu}{R^3}y_L + a_y \\
\ddot{z} &= -\frac{2\mu}{R^3}y + a_z
\end{aligned} \tag{4}$$

If the first satellite has a circular orbit (R=a), its angular acceleration is zero ($\ddot{\varphi}_R = 0$), then its mean motion can be expressed by

$$\dot{\varphi}_R = n = \sqrt{\frac{\mu}{a^3}} \tag{5}$$

and the linear system of equations with constant coefficients, called Hill-Clohessy-Wiltshire (HCW), is obtained as follows

$$\begin{aligned}
\ddot{x}_c - 2n\dot{y}_c - 3n^2 x_c &= a_x \\
\ddot{y}_c + 2n\dot{x}_c &= a_y \\
\ddot{z}_c + n^2 z_c &= a_z.
\end{aligned} \tag{6}$$

These equations describe the movement of the main satellite with respect to the target satellite for circular orbit and small deviations. For constant accelerations a_x, a_y, and a_z, this system of equations can be solved analytically [17]. The solution of the non-homogenous system of equations () is

$$x_c(t) = \left[x_c(t_0) + \frac{1}{3n^2} a_x \right](4 - 3\cos n(t-t_0)) +$$
$$\left[\frac{\dot{x}_c(t_0)}{n} - \frac{2a_y}{n^2} \right] \sin n(t-t_0) +$$
$$+ \frac{2\dot{y}_c(t_0)}{n}(1 - \cos n(t-t_0)) - \frac{1}{3n^2} a_x + 2\frac{a_y}{n}(t-t_0)$$
$$y_c(t) = y_c(t_0) + \dot{y}_c(t_0)\left[\frac{4}{n} \sin n(t-t_0) - 3(t-t_0) \right] +$$
$$+6\left[x_c(t_0) + \frac{1}{3n^2} a_x \right]\left[\sin n(t-t_0) - n(t-t_0) \right] +$$
$$+2\left[\frac{\dot{x}_c(t_0)}{n} - \frac{2a_y}{n^2} \right](\cos n(t-t_0) - 1) - \frac{3}{2} a_y (t-t_0)^2$$
$$z_c(t) = \left[z_c(t_0) - \frac{1}{n^2} a_z \right] \cos n(t-t_0) + \frac{\dot{z}_c(t_0)}{n} \sin n(t-t_0) + \frac{1}{n^2} a_z \quad (7)$$

Where $x_c(t_0)$, $y_c(t_0)$, $z_c(t_0)$, $\dot{x}_c(t_0)$, $\dot{y}_c(t_0)$ and $\dot{z}_c(t_0)$ are the initial conditions. The HCW model does not include neither perturbations nor the eccentricity of the orbit.

LINEAR MODEL FOR SMALL ECCENTRICITY

Nonlinear equations () are valid for Keplerian orbits without any disturbances, their linearized version () for circular (eccentricity $\varepsilon = 0$) orbits only. In this section the influence of non-zero eccentricity will be investigated by the method of small deviations (perturbations). First a linear model of equations of the target satellite movement (Eqns. ,) will be obtained for small ε by linearization of orbit deviations from the circular orbit. Next the influence of these deviations on relative position of a satellite will be investigated.

Linearization of the orbit

First a linear model of deviations from circular orbit will be developed for small ε. The distance of the target satellite to the Earth centre point and the time derivative of its true anomaly can be expressed as deviations from the semi major axis of the motion ellipse *a* and its mean motion *n* respectively, so they can be expressed as

$$R = a + \Delta R$$
$$\dot{\varphi} = n + \Delta\dot{\varphi} \quad . \quad (8)$$

According to the method of perturbations the deviations are expressed as

$$\Delta R = \varepsilon R_1$$
$$\Delta\dot{\varphi} = \varepsilon\dot{\varphi}_1 \quad (9)$$

Introducing Eqns. () and , Eqns () and () become

$$\varepsilon\ddot{R}_1 = (a + \varepsilon R_1)(n + \varepsilon\dot{\varphi}_1) - \frac{\mu}{(a + \varepsilon R_1)^2} \quad (10)$$

$$\varepsilon\ddot{\varphi}_1 = -\frac{2\varepsilon\dot{R}_1(n + \varepsilon\dot{\varphi}_1)}{a + \varepsilon R_1} \quad (11)$$

and with expanding the fractions into Taylor series

$$\varepsilon\ddot{R}_1 = an^2 + 2an\varepsilon\dot{\varphi}_1 + \varepsilon n^2 R_1 + 2\varepsilon^2 R_1 n\dot{\varphi}_1 +$$
$$+\varepsilon^3 R_1\dot{\varphi}_1^2 - \frac{\mu}{a^2}(1 - 2\varepsilon\frac{R_1}{a} + ...) \quad (12)$$

$$\varepsilon\ddot{\varphi}_1 = -\frac{2\varepsilon\dot{R}_1}{a}(n + \varepsilon n\frac{R_1}{a} + \varepsilon\dot{\varphi}_1 + \varepsilon^2(...)) \quad (13)$$

Collecting the terms with ε and observing Eq. (5), we get two linear equations for R_1 and $\dot{\varphi}_1$

$$\ddot{R}_1 = 2an\dot{\varphi}_1 + 3n^2 R_1 \quad (14)$$

$$\ddot{\varphi}_1 = -\frac{2n}{a}\dot{R}_1 \quad (15)$$

Next initial conditions for $R_1, \dot{R}_1$ and $\dot{\varphi}_1$ will be developed. It is supposed that the time starts $(t = 0)$ when the leader (target) satellite passes the perigee and so its true anomaly $\varphi(0)$ is zero and its distance to the Earth mass point is

$$R(0) = a - f = a(1 - \varepsilon) \quad , \quad (16)$$

where *f* is the distance from the centre of the ellipse to the focus. From this equation it follows

$$\Delta R(0) = -a\varepsilon \rightarrow R_1(0) = -a \quad (17)$$

At the perigee, *R* has its minimum, so

$$\dot{R} = \Delta\dot{R} = 0 \rightarrow R_1(0) = 0 \tag{18}$$

Using well known equations for the true (φ) mean (M) and eccentric (E) anomaly

$$M = n \cdot t = E - \varepsilon \sin E \tag{19}$$

$$d\varphi = \frac{\sqrt{1-\varepsilon^2}}{1-\varepsilon\cos E} dE \tag{20}$$

we get for $t = 0$ that $\varphi(0) = E(0) = 0$ and

$$\left.\frac{dM}{dt}\right|_{t=0} = n = (1-\varepsilon\cos E)\left.\frac{dE}{dt}\right|_{t=0} = (1-\varepsilon)\left.\frac{dE}{dt}\right|_{t=0} \tag{21}$$

and consequently

$$\frac{d\varphi(0)}{dt} = \dot{\varphi}(0) = \frac{\sqrt{1-\varepsilon^2}}{(1-\varepsilon)^2} n \tag{22}$$

.

Using () and expanding () into Taylor series we get

$$\Delta\dot{\varphi}(0) = \dot{\varphi}(0) - n = (\frac{\sqrt{1-\varepsilon^2}}{(1-\varepsilon)^2} - 1)n = 2n\varepsilon + \frac{5}{2} n\varepsilon^2 + ... \tag{23}$$

Considering only the first term of Eq. , the initial condition for $\dot{\varphi}_1$ is obtained as follows:

$$\dot{\varphi}_1(0) = 2n \tag{24}$$

Equations have an analytical solution which will be developed next using the derived initial conditions (), () and . The integration of Eq. yields

$$\dot{\varphi}_1 = -\frac{2n}{a}(R_1 - R_1(0)) + \dot{\varphi}_1(0) = \\ = -\frac{2n}{a}(R_1 + a) + 2n = -\frac{2n}{a} R_1 \tag{25))}$$

Eq. now becomes

$$\ddot{R}_1 = 2an(-\frac{2n}{a} R_1) + 3n^2 R_1 = -n^2 R_1 \tag{26}$$

and its solution with respect to initial conditions (), () is

$$R_1(t) = -a\cos nt \tag{27}$$

Eq. now becomes

$$\dot{\varphi}_1 = -\frac{2n}{a}(-a\cos nt) = 2n\cos nt \tag{28}$$

The deviations ΔR and $\Delta\dot{\varphi}$ now become:

$$\Delta R(t) = -\varepsilon a\cos nt \\ \Delta\dot{\varphi}(t) = -\frac{2n}{a}(-\varepsilon a\cos nt) = 2n\varepsilon\cos nt \tag{29}$$

Equations () represent the analytical solution of the linear deviation model with respect to derived initial conditions.

Linearization of the velocity

Due to changing radius of the orbit and changing radial velocity, also the linear velocity of the main satellite is changed and will be elaborated next.

The orbital velocity of the main satellite is

$$v(t) = R(t)\dot{\varphi}(t) = a(1-\varepsilon\cos nt)\cdot n(1+2\varepsilon\cos nt) = \\ = an(1+\varepsilon\cos nt) + O(\varepsilon^2) \tag{30}$$

where the term with ε^2 will be neglected. Introducing

$$v(t) = v_0(t) + \Delta v(t) \tag{31}$$

The nominal velocity v_0 and the deviation of the velocity Δv are

$$v_0(t) = an = \sqrt{\frac{\mu}{a}} \\ \Delta v(t) = an\varepsilon\cos nt \tag{32}$$

Next the influence of all above given deviations on the deviations of relative distance of satellites will be investigated.

Application of the method of perturbations to the formation flying model

By the method of perturbations, the deviations from the solutions for circular orbit are described by

$$\Delta x(t) = \varepsilon x_1(t) \\ \Delta y(t) = \varepsilon y_1(t) \\ \Delta z(t) = \varepsilon z_1(t) \tag{33}$$

where ε is a small parameter. In our case the eccentricity ε, which is supposed to be small, will be used. The *x, y* and *z* components for the perturbed model now become

$$x_p(t) = x_c(t) + \Delta x(t) = x_c(t) + \varepsilon x_1(t)$$
$$y_p(t) = y_c(t) + \Delta y(t) = y_c(t) + \varepsilon y_1(t) \qquad (34)$$
$$z_p(t) = z_c(t) + \Delta z(t) = z_c(t) + \varepsilon z_1(t)$$

Linear equations with time varying parameters. can now be written using Eqns. (34), (), () as follows

$$(\ddot{x}_c + \varepsilon\ddot{x}_1) - 2(n + 2n\varepsilon\cos nt)(\dot{y}_c + \varepsilon\dot{y}_1) +$$
$$+2n^2\varepsilon\sin nt(y_c + \varepsilon y_1) -$$
$$-(n + 2n\varepsilon\cos nt)^2(x_c + \varepsilon x_1) = \frac{2\mu(x_c + \varepsilon x_1)}{a^3(1-\varepsilon\cos nt)^3} + a_x \qquad (35)$$

$$(\ddot{y} + \varepsilon\ddot{y}_1) + 2(n + 2n\varepsilon\cos nt)(\dot{x}_c + \varepsilon\dot{x}_1) -$$
$$-2n^2\varepsilon\sin nt(x_c + \varepsilon x_1) -$$
$$-(n + 2n\varepsilon\cos nt)^2(y_c + \varepsilon y_1) = \frac{2\mu(y_c + \varepsilon y_1)}{a^3(1-\varepsilon\cos nt)^3} + a_y \qquad (36)$$

$$\ddot{z}_c + \varepsilon\ddot{z}_1 = -\frac{z\mu(z_c + \varepsilon z_1)}{a^3(1-\varepsilon\cos nt)^3} + a_z \qquad (37)$$

Collecting the left hand side of these equations with respect to ε and expanding the right hand side into Taylor series, we get

$$\ddot{x}_c - 2n\dot{y}_c - n^2x_c + \varepsilon(\ddot{x}_1 - 4n\dot{y}_c\cos nt - 2n\dot{y}_1 +$$
$$+2n^2y_c\sin nt - n^2x_1 - 4n^2x_c\cos nt) +$$
$$+\varepsilon^2(...) + \varepsilon^3(...) + ... =$$
$$= 2n^2(x_c + \varepsilon x_1)(1 + \varepsilon 3\cos nt + \varepsilon^2(...) + ...) =$$
$$= 2n^2x_c + \varepsilon(2n^2x_1 + 6n^2x_c\cos nt) +$$
$$+\varepsilon^2(...) + \varepsilon^3(...) + ... + a_x \qquad (38)$$

$$\ddot{y}_c + 2n\dot{x}_c - n^2y_c + \varepsilon(\ddot{y}_1 - 4n\dot{x}_c\cos nt + 2n\dot{x}_1 -$$
$$-2n^2x_c\sin nt - n^2y_1 - 4n^2y_c\cos nt) +$$
$$+\varepsilon^2(...) + \varepsilon^3(...) + ... =$$
$$= -n^2(y_c + \varepsilon y_1)(1 + \varepsilon 3\cos nt + \varepsilon^2(...) + ...) =$$
$$= -n^2y_c + \varepsilon(-n^2y_1 - 3n^2y_c\cos nt) +$$
$$+\varepsilon^2(...) + \varepsilon^3(...) + ... + a_y \qquad (39)$$

$$\ddot{z}_c + \varepsilon\ddot{z}_1 = -n^2(1 + 3\varepsilon\cos nt)(z_c + \varepsilon z_1) +$$
$$+\varepsilon^2(...) + \varepsilon^3(...) + ... =$$
$$= -n^2z_c - \varepsilon(n^2z_1 + 3n^2z\cos nt) + \qquad (40)$$
$$+\varepsilon^2(...) + \varepsilon^3(...) + ... + a_z$$

The terms without ε represent the original system of equations for circular orbit (6) while the terms with ε represent a new system of equations for x_1, y_1 and z_1, respectively. The terms with higher exponents will be neglected.

The system of equations for x_1 ,y_1 and z_1 now becomes

$$\ddot{x}_1 - 2n\dot{y}_1 - 3n^2x_1 =$$
$$= (10n^2x_c + 4n\dot{y}_c)\cos nt - 2n^2y_c\sin nt \qquad (41)$$

$$\ddot{y}_1 + 2n\dot{x}_1 = (-4n\dot{x}_c + 4n^2y_c - 3n^2yc)\cos nt =$$
$$= (n^2y_c - 4n\dot{x}_c)\cos nt + 2n^2x_c\sin nt \qquad (42)$$

$$\ddot{z}_1 + n^2z_1 = -3n^2z_c\cos nt. \qquad (43)$$

The initial conditions for deviations are obtained under presumption that the centre of the elliptical orbit remains in the centre of the circular orbit as follows

$$x_1(0) = z_1(0) = 0$$
$$y_1(0) = y_0 \qquad (44)$$

Due to the eccentricity of the orbit, the Along-track initial distance y_0 causes velocity changes in the Radial and In-track directions. Due to the In-track distance y_0, the satellites are flying along the same track however they pass the perigee with a time shift of Δt

$$\Delta t = \frac{y_0}{R(0)\dot{\phi}(0)} = \frac{y_0}{an(1+\varepsilon)} \approx \frac{y_0}{an} \qquad (45)$$

The initial velocities for deviations are then

$$\dot{x}_1(0) = \dot{R}_1(\Delta t) - \dot{R}_1(0) =$$
$$= an\sin n\Delta t \approx an^2\Delta t = ny_0$$
$$\dot{y}_1(0) = \Delta v(\Delta t) - \Delta v(0) = \qquad (46)$$
$$= an\varepsilon\cos n\Delta t - an\varepsilon\cos 0 \approx 0$$
$$\dot{z}_1(0) = 0$$

The linear model for small eccentricities is given by equations (41), (42), (43) with initial conditions (44) and (45).

ANALYTICAL SOLUTION OF THE LINEAR MODEL FOR SMALL ECCENTRICITY

Deviations for the cross-track motion are decoupled from the deviation of the radial and in-track motion so both motions will be treated separately. First the deviations for the in-track-and radial motion will be solved analytically for different manoeuvres which actually correspond to different initial conditions. Since the model is linear, the solution for combined initial condition is the sum of the solutions for individual initial conditions.

Initial Radial displacement

This manouevre corresponds to the radial parallel flying (drifting); without continuous acceleration the satellites can not fly in this constellation for a long time. The analytical solution of Eqns. (41), (42) with initial conditions (44) (46) considering $y_0 = 0,\ \dot{x}_0 = \dot{y}_0 = 0$ describes the deviations of the orbit of the main satellite relative to the target from the motion, which is the solution of the HCW equations (1) and is as follows

$$x_1 = 6x_0 \sin\left(nt - \frac{nt_0}{2}\right)^2 - 24x_0 \sin\left(\frac{nt}{2} - \frac{nt_0}{2}\right)^2 - \\ -12x_0 \sin\left(\frac{nt}{2} + \frac{nt_0}{2}\right)^2 + 56x_0 \sin\left(\frac{nt}{2}\right)^2 + \\ +30x_0 \sin\left(\frac{nt_0}{2}\right)^2 - 6nt\,x_0 \sin(nt)$$

$$y_1 = \frac{9x_0}{2}\sin(2nt - nt_0) + 48x_0 \sin(nt) - \\ -\frac{15x_0}{2}\sin(nt_0) + 12x_0 \sin(nt_0)\cos(nt) - \\ -36x_0 \cos(nt_0)\sin(nt) - 42nt\,x_0 + 6nt_0\,x_0 - \\ -6nt\,x_0 \cos(nt) + 27nt\,x_0 \cos(nt_0) - \\ -6nt_0\,x_0 \cos(nt) \qquad (47)$$

Where x_0 is the initial displacement of the main satellite in the target satellite co-ordinate system and t_0 is the initial time. If the manoeuvre starts at perigee $(t_0 = 0)$ or at apogee $(t_0 = \pi/n)$ or mean anomaly of 90^0 $(t_0 = \pi/(2n))$. or mean anomaly of 270^0 $(t_0 = 3\pi/(2n))$, these equations become

$$x_1 = 2x_0\left(3\sin(nt)^2 - 3nt\sin(nt) + 10\sin\left(\frac{nt}{2}\right)^2\right)$$

$$y_1 = 3x_0\left(4\sin(nt) - 5nt + 3\cos(nt)\sin(nt) - \right. \\ \left. -2nt\cos(nt)\right) \qquad (48)$$

Initial In-track displacement

This manouevre corresponds to the along track parallel flying. The analytical solution of Eq. (41), (42) with initial conditions (44), (46) considering $x_0 = \dot{x}_0 = \dot{y}_0 = 0$ is

$$x_1 = y_0 \sin(nt) \qquad (49)$$

$$y_1 = y_0 \cos(nt) \qquad (50)$$

The follower is not flying in constant displacement to the main, as it is in a circular orbit; rather, it is circulating around this point on a circle with radius, y_0. The solution does not depend on the initial time.

Initial Radial velocity

This manouevre corresponds to the circumvolution of a point on the orbit of the target satellite. The analytical solution of Eq. (41), (42) with initial conditions (44), (46) considering $x_0 = y_0 = 0,\ \dot{y}_0 = 0$ describes the deviations of the orbit of the main satellite relative to the target from the ellipse, which is the solution of the HCW equations (1) and is as follows

$$x_1 = \frac{\dot{x}_0}{n}\left(2\sin(nt + nt_0) - 4\sin(nt - nt_0)\right. \\ \left. + \sin(2nt - nt_0) - 5\sin(nt_0)\right)$$

$$y_1 = 9t\,\dot{x}_0 \sin(nt_0) - \frac{\dot{x}_0}{2n}\left(6\sin\left(nt - \frac{nt_0}{2}\right)^2 - \right. \\ -32\sin\left(\frac{nt}{2} - \frac{nt_0}{2}\right)^2 + 16\sin\left(\frac{nt}{2} + \frac{nt_0}{2}\right)^2 + \\ \left. +8\sin\left(\frac{nt}{2}\right)^2 + 10\sin\left(\frac{nt_0}{2}\right)^2\right) \qquad (51)$$

If the manoeuvre starts at perigee ($t_0 = 0$) these equations become

$$x_1 = -\frac{4\dot{x}_0}{n}\sin(nt)\sin\left(\frac{nt}{2}\right)^2$$
$$y_1 = -\frac{\dot{x}_0}{n}\left(3\sin(nt)^2 - 4\sin\left(\frac{nt}{2}\right)^2\right) \quad (52)$$

If the manoeuvre starts at apogee ($t_0 = \pi/n$) these equations become

$$x_1 = \frac{2\dot{x}_0}{n}\sin(nt) - \dot{x}_0\sin(2nt) - y0\sin(nt)$$
$$y_1 = -\frac{7\dot{x}_0}{n} + \frac{6\dot{x}_0}{n}\cos(nt) + \frac{\dot{x}_0}{n}\cos(nt)^2 + \frac{4\dot{x}_0}{n}\sin(nt)^2 \quad (53)$$

If the manoeuvre starts at the true anomaly of 90^0 ($t_0 = \pi/(2n)$), equations for deviations become

$$x_1 = \frac{2\dot{x}_0}{n}\sin(nt)^2 - \frac{12\dot{x}_0}{n}\sin\left(\frac{nt}{2}\right)^2$$
$$y_1 = 9t\dot{x}_0 - \frac{12\dot{x}_0}{n}\sin(nt) - \frac{4\dot{x}_0}{n}\sin\left(\frac{nt}{2}\right)^2 + \frac{3\dot{x}_0}{n}\cos(nt)\sin(nt) \quad (54)$$

If the manoeuvre starts at the true anomaly of 270^0 ($t_0 = 3\pi/(2n)$), equations for deviations become

$$x_1 = \frac{12\dot{x}_0}{n}\sin\left(\frac{nt}{2}\right)^2 - \frac{2\dot{x}_0}{n}\sin(nt)^2$$
$$y_1 = \frac{12\dot{x}_0}{n}\sin(nt) - 9t\dot{x}_0 - \frac{4\dot{x}_0}{n}\sin\left(\frac{nt}{2}\right)^2 - \frac{3\dot{x}_0}{n}\cos(nt)\sin(nt) \quad (55)$$

Initial In-track velocity

This manouevre corresponds to the change of the In-track displacement. The analytical solution of Eq. (41), (42) with initial conditions (44), (46) considering $x_0 = y_0 = 0,\ \dot{x}_0 = 0$ describes the deviations of the orbit of the main satellite relative to the target from the motion, which is the solution of the HCW equations (1) and is as follows

$$x_1 = \frac{1}{n}\left[\dot{y}_0(4\cos(nt + nt_0) + 8\cos(nt - nt_0) - 2\cos(2nt - nt_0) - 14\cos(nt) - 10\cos(nt_0) + 14)\right] - 3t\dot{y}_0\sin(nt)$$
$$y_1 = 3t_0\dot{y}_0 - 21t\dot{y}_0 + \frac{24\dot{y}_0}{n}\sin(nt) - \frac{5\dot{y}_0}{n}\sin(nt_0) - 3t\dot{y}_0\cos(nt) + 18t\dot{y}_0\cos(nt_0) - 3t_0\dot{y}_0\cos(nt) - \frac{8\dot{y}_0}{n}\sin(nt + nt_0) - \frac{16\dot{y}_0}{n}\sin(nt - nt_0) + \frac{3\dot{y}_0}{n}\sin(2nt - nt_0) \quad (56)$$

If the manoeuvre starts at perigee ($t_0 = 0$) these equations become

$$x_1 = \frac{\dot{y}_0}{n}\left(4\sin(nt)^2 + 4\sin\left(\frac{nt}{2}\right)^2\right) - 3t\dot{y}_0\sin(nt)$$
$$y_1 = \frac{3\dot{y}_0}{n}\sin(2nt) - 3\dot{y}_0\left(t + t\cos(nt)\right) \quad (57)$$

If the manoeuvre starts at apogee ($t_0 = \pi/n$) these equations become

$$x_1 = -3t\dot{y}_0\sin(nt) - \frac{\dot{y}_0}{n}\left(4\sin(nt)^2 - 52\sin\left(\frac{nt}{2}\right)^2\right)$$
$$y_1 = -\frac{3\dot{y}_0}{n}\left(\sin(2nt) - 16\sin(nt) - \pi + 13nt + \pi\cos(nt) + nt\cos(nt)\right) \quad (58)$$

If the manoeuvre starts at the true anomaly of 90^0 ($t_0 = \pi/(2n)$), equations for deviations become

$$x_1 = \frac{28\dot{y}_0}{n}\sin\left(\frac{nt}{2}\right)^2 - 3t\dot{y}_0\sin(nt) + \frac{8\dot{y}_0}{n}\sin(nt)\sin\left(\frac{nt}{2}\right)^2$$

$$y_1 = \frac{\dot{y}_0}{n}\left(24\sin(nt) + 6\sin(nt)^2 - 16\sin\left(\frac{nt}{2}\right)^2 \right.$$
$$\left. - 24nt + 3\pi\sin\left(\frac{nt}{2}\right)^2 + 6nt\sin\left(\frac{nt}{2}\right)^2 \right) \quad (59)$$

If the manoeuvre starts at the true anomaly of 270^0 $(t_0 = 3\pi/(2n))$, equations for deviations become

$$x_1 = \frac{28\,\dot{y}_0}{n}\sin\left(\frac{nt}{2}\right)^2 - 3t\,\dot{y}_0\sin(nt) -$$
$$- \frac{8\,\dot{y}_0}{n}\sin(nt)\sin\left(\frac{nt}{2}\right)^2 \quad (60)$$
$$y_1 = \frac{\dot{y}_0}{n}\left(24\sin(nt) - 6\sin(nt)^2 + 16\sin\left(\frac{nt}{2}\right)^2 - \right.$$
$$\left. - 24nt + 9\pi\sin\left(\frac{nt}{2}\right)^2 + 6nt\sin\left(\frac{nt}{2}\right)^2 \right)$$

Cross-track deviations

The deviations of orbit of the main satellite relative to the target from the sinusoidal motion, which is the solution of the HCW equations (1) is the solution of Eq. (43) with initial conditions (44) and (46) and is as follows

$$z_1(t) = z(t_0)\cos(nt + nt_0) + \frac{z(t_0)}{2}\cos(2nt - nt_0) +$$
$$+ \frac{1}{n}\left[\frac{\dot{z}(t_0)}{2}\sin(2nt - nt_0) - \dot{z}(t_0)\sin(nt + nt_0) + \right.$$
$$\left. + \frac{3}{2}\dot{z}(t_0)\sin(nt_0)\right] - \frac{3}{2}z(t_0)\cos(nt_0) \quad (61)$$

If the manoeuvre starts at perigee $(t_0 = 0)$ these equations become

$$z_1(t) = -z(t_0)\sin(nt)^2 - 2\,z(t_0)\sin\left(\frac{nt}{2}\right)^2 -$$
$$- \frac{2\,\dot{z}(t_0)}{n}\sin(nt)\sin\left(\frac{nt}{2}\right)^2 \quad (62)$$

If the manoeuvre starts at apogee $(t_0 = \pi/n)$ these equations become

$$z_1(t) = \frac{\dot{z}(t_0)}{n}\left(\sin(nt)^2 + 2\sin\left(\frac{nt}{2}\right)^2 \right) -$$
$$- 2\,z(t_0)\sin(nt)\sin\left(\frac{nt}{2}\right)^2 \quad (63)$$

If the manoeuvre starts at the true anomaly of 90^0 $(t_0 = \pi/(2n))$, equations for deviations become

$$z_1(t) = \frac{\dot{z}(t_0)}{n}\left(\sin(nt)^2 + 2\sin\left(\frac{nt}{2}\right)^2 \right) -$$
$$- 2\,z(t_0)\sin(nt)\sin\left(\frac{nt}{2}\right)^2 \quad (64)$$

If the manoeuvre starts at the true anomaly of 270^0 $(t_0 = 3\pi/(2n))$, equations for deviations become

$$z_1(t) = 2\,z(t_0)\sin(nt)\sin\left(\frac{nt}{2}\right)^2 -$$
$$- \frac{\dot{z}(t_0)}{n}\left(\sin(nt)^2 + 2\sin\left(\frac{nt}{2}\right)^2 \right) \quad (65)$$

VALIDATION OF THE MODELS AGAINST THE PRISMA EXPERIMENT

In this section the experimental data acquired during in-flight simulated radar interferometry propagation will be used to evaluate and compare the models with respect to how they capture relative dynamics of the satellites considering different phenomena, such as orbit eccentricity and Earth oblateness. The experimental measurements have been improved by Precise Orbit Determination (POD) [18]. It should be noted that the models are not compared with respect to their ability to predict the relative propagation but with the repect to their ability to cope various phenomena, such as e.g. Earth oblateness etc.

The experiment was performed on September 19, 2011 from 3 to 9 am UTC. The data used for the evaluation start in the Tango perigee, at 03:18:20 and ends at 08:14:20 with the sampling time of 10*s*. The precision of the relative position with POD data is 2 cm, 3D, rms.

During this experiment Mango was flown without trajectory control, the safety box for Mango was set to 10m. In an ideal case (HCW model, zero relative initial velocity) the satellites would fly in constant in-track distance. However the experiment exhibits some

periodic motion and a parabolic drift, which are due to an elliptical orbit, nonzero initial conditions and real environment. To eliminate the influence of initial conditions, the models were individually optimized. We believe that the parabolic drift was due to the difference of the drag of both satellites. In order to eliminate it, a constant acceleration in the in-track direction was added to Mango. Initial relative positions, initial relative velocities and a constant in-track acceleration were obtained by means of optimisation.

There was a slight cross-track sinusoidal movement of Mango in Tango's RIC co-ordinate system with amplitude of 57cm. All models cope with this movement within an error of 16mm which is below the precision of the POD data. So only the Radial/In-track models will be evaluated.

The optimization was performed in Matlab using function `fminsearch` with the cost function equal to the average distance of the model response to the POD data

$$D = \sqrt{\frac{1}{N}\sum_{i=0}^{N}\left(\left(x_i - x_i^m\right)^2 + \left(y_i - y_i^m\right)^2 + \left(z_i - z_i^m\right)^2\right)}$$

where x_i, y_i, z_i are the POD data and x_i^m, y_i^m, z_i^m are the model data. N is the number of data. As described above only the projection of the results into the orbit plane will be presented; the influence of the cross-track movement was negligible. The optimal initial conditions for various models are given in Table I, while Table II presents the optimal values of the cost function D. Table III exposes the acceleration needed to compensate the parabolic drift. The meaning of the abreviations in all tables is as follows: HCW = Hill-Clohessy-Wiltshire, Non_LIN = non-linear model, Lin-Pert = Linear model derived by the method of perturbation, STK-EMP = STK Earth Mass Point, STK-J2 = STK J2, STK-HPOP-d = STK High Precision Orbit Propagator with default settings, STK-HPOP-a = STK High Precision Orbit Propagator with all disturbances included.

Figure 9 represents the projection of the relative Mango orbit into the Tango orbital plane for various models with the same designation as in the Tables. Figures 10 and 11 depict radial and in-track deviations of the model response to the POD data respectively for various models.

From presented results it is obvious that there are three groups of models.

Table I: Optimal initial conditions for various models

	$x(t_0)$ [m]	$y(t_0)$ [m]	$\dot{x}(t_0)$ [mm/s]	$\dot{y}(t_0)$ [mm/s]
HCW	-0.8259	198.4031	-1.1112	1.7052
Non-Lin	-0.8313	198.2495	-0.7931	1.6396
Lin-Pert	-0.8289	197.5694	-1.5415	1.7187
STK-EMP	-0.8078	198.2876	-0.8321	1.7137
STK-J2	-0.8675	198.1536	-0.6074	1.6449
STK-HPOP-d	-0.8671	198.1539	-0.6056	1.6427
STK-HPOP-a	-0.8673	198.1534	-0.6047	1.6429

Table II. Optimal values for the cost function D for various methods.

Model	HCW	Non-Lin	Lin-Pert	STK-EMP
D	0.2515	0.1308	0.1292	0.1307
Model	STK-J2	STK-HPOP-d	STK-HPOP-a	
D	0.1312	0.1326	0.1326	

Table III: Accelerations needed to compensate the parabolic drift.

Model	HCW	Non-Lin	Lin-Pert	STK-EMP
a_y [10^{-9} m/s^2]	7.109	7.287	7.316	6.779
Model	STK-J2	STK-HPOP-d	STK-HPOP-a	
a_y [10^{-9} m/s^2]	7.569	7.559	7.580	

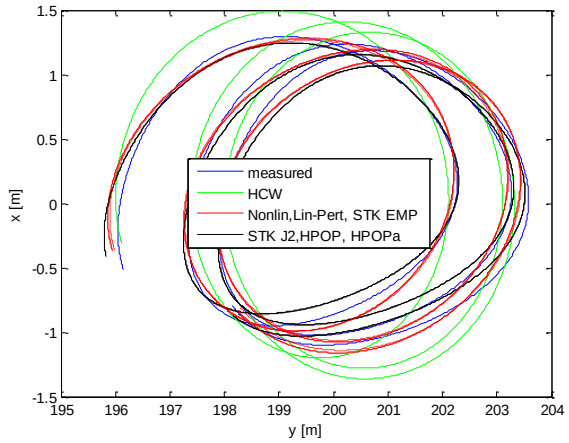

Fig. 9: The projection of the relative Mango orbit into the Tango orbital plane for various models.

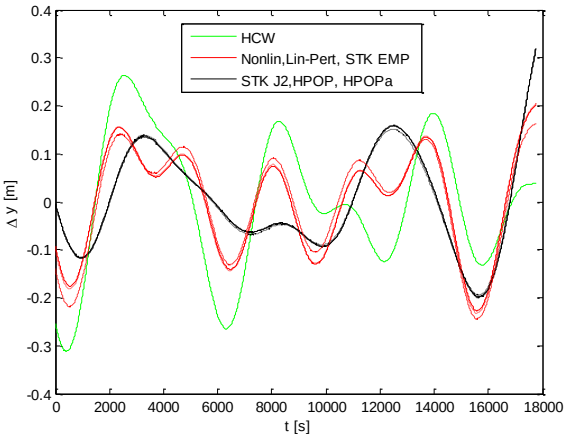

Fig. 11: In-track deviations of the model response to the POD data for various models.

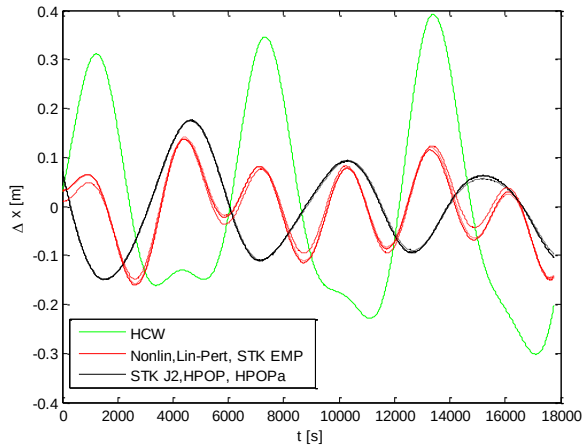

Fig. 10: Radial deviations of the model response to the POD data for various models.

In the first group there is the simple HCW model (represented in solid green) with the worst cost function and greatest deviations. The first harmonic deviations in this model are the consequence of orbit eccentricity.

In the second group there are the non-linear model (dotted), the STK Earth Mass Point model (dashed) and the newly developed (by the method of perturbations) linear model (solid). All three models are presented in red colour. It should be noted that the non-linear and the STK-EMP model are theoretically identical and that the newly developed linear model is very similar to them due to the small eccentricity of the Prisma orbits (0.004). Second harmonic deviations can be observed, which are due to the oblateness of the Earth. STK J2 and High Precision Orbit Propagator models form the third group. It can be observed that they eliminated the effect of the Earth oblateness.

Obviously the HPOP propagators (default settings and with all disturbances included) do not exhibit any improvement of the model. In all STK models a numerical noise can be observed too. It can be concluded that the newly developed linear model for orbits with small eccentricities can cope with this phenomenon adequately and mitigates for the shortcomings of the currently widely used model sets.

Conclusion

Three sets of experiments performed by SPACE-SI and OHB Sweden in September 2011 with Prisma satellites are presented. They include the in-flight simulated radar interferometry, the observation of non-cooperative objects - space debris and the in-flight simulated distributed instrument experiment. A collateral outcome of close debris observation from an orbit, which is encircling the target by its natural motion, were also images of interesting areas (Kuwait, Djibouti, Crete) in the background. The timing of acquisition was precisely calculated in order to capture both targets simultaneously. The in-flight simulated distributed instrument experiment included alignment of Mango and Tango satellites with the predefined locations on the Earth (Piran, Cape Town, Punta Arenas). The successful positioning of the satellites during the is demonstrated by satisfactory pictures although imaging conditions were not favourable due to the very unsuitable dusk-dawn orbit, autumnal equinox time slot and bad weather.

Several formation flying models are reviewed, such as nonlinear model and its linearization − the HCW model. An extension of the linear HCW model to orbits with small eccentricities is derived by the method of perturbations. The obtained model is linear with time

varying parameters (depending on the target's satellite true anomaly).

The astrodynamic data of the in flight simulated radar interferometry remote-sensing experiment were used to verify several formation flying models including a nonlinear model, a linear Hill-Clohessy-Wiltshire model, STK models with four propagators (Earth mass point, J2, default HPOP and HPOP with all disturbances) and the hereby originally proposed extension to the Hill-Clohessy-Wiltshire model, a linear model for orbits with small eccentricities, which can cope with the phenomenon of eccentricity adequately and mitigates for the shortcomings of the currently widely used model sets.

Acknowledgments

The Centre of Excellence for Space Sciences and Technologies SPACE-SI is an operation partly financed by the European Union, European Regional Development Fund and Republic of Slovenia, Ministry of Higher Education, Science and Technology.

Authors appreciate the help of DLR Oberpfaffenhofen, Germany for providing the POD data.

References

1. Persson S., Jacobsson B., Gill E., PRISMA - Demonstration Mission for Advanced Rendevouz and Formation Flying Technologies and Sensors, Proceedings of the 56th International Astronautical Congress (IAC-05-B5.6.B.07), Fukuoka, Japan, October 2005
2. Persson S., Jacobsson B., "PRISMA - Swedish in-orbit testbed for rendezvous and formation flying," Proceedings of the 57th IAC/IAF/IAA (International Astronautical Congress), Valencia, Spain, Oct. 2-6, 2006, IAC-06-D1.2.02
3. Larsson R., Berge S., Bodin P., Jönsson U., Fuel Efficient Relative Orbit Control Strategies for Formation Flying and Rendezvous within PRISMA, 29th ANNUAL AAS GUIDANCE AND CONTROL CONFERENCE, Colorado February 4-8, 2006
4. http://ohb-sweden.se/Prisma
5. S.R.Ploen, D.P. Scharf, F.Y. Hadaegh and A.B. Acikmese, Dynamics of Earth Orbiting Formations, http://trs-new.jpl.nasa.gov/dspace/bitstream /2014/38974/1/04-1594.pdf
6. D. R. Izzo, Formation Flying Linear Modelling, in: Dynamics of Systems and Structures in Space, 5th conference, Kings College, Cambridge, July 2002
7. J. Richards. Remote Sensing with Imaging Radar. Springer, 2009.
8. Krieger, G.; Moreira, A.; Fiedler, H.; Hajnsek, I.; Werner, M.; Younis, M.; Zink, M.; , "TanDEM-X: A Satellite Formation for High-Resolution SAR Interferometry," Geoscience and Remote Sensing, IEEE Transactions on , vol.45, no.11, pp.3317-3341, Nov. 2007.
9. Y. T. Yoon, M. Eineder, N. Yague-Martinez, and O. Montenbruck, "TerraSAR-X precise trajectory estimation and quality assessment," IEEE Trans. Geosci. Remote Sens., vol. 47, no. 6, pp. 1859–1868, Jun. 2009
10. R. Romeiser and D. R. Thompson, "Numerical study on the along-track interferometric radar imaging mechanism of oceanic surface currents," IEEE Trans. Geosci. Remote Sens., vol. 38, no. 1, pp. 446–458, Jan. 2000
11. C. Reigber, Y. Xia, H. Kaufmann, T. Timmen, J. Bodechtel, and M. Frei, "Impact of precise orbits on SAR interferometry," in Proc. FRINGE 96 Workshop, Zurich, Switzerland, 1996.
12. D. Matko et. all., SPACE-SI Formation Flying Experiments on Prisma Satellites, Proceedings of the 4S Symposium, Portorož, Slovenia, 2012.
13. C. Chasset, S. Berge, P. Bodin, B. Jakobsson, 3-axis Magnetic Control with Multiple Attitude Profile Capabilities in the PRISMA Mission, Space Technology, Vol. 26, Issue 3-4, 2007, pp 137-154.
14. http://www.stoff.pl/
15. www.mathworks.com
16. www.agi.com
17. MATKO, Drago, RODIČ, Tomaž, OŠTIR, Krištof, MARSETIČ, Aleš, PELJHAN, Marko, BLAŽIČ, Sašo, KLANČAR, Gregor, MUŠIČ, Gašper. Optimization of fuel consumption with respect to orbital requirements for high resolution remote sensing satellite constellations. V: 25th Annual AIAA/USU Conference on Small Satellites, Aug. 8-11 2011, Logan, Utah, USA
18. D'Amico S., Ardaens J.-S., Larsson R.;Spaceborne Autonomous Formation Flying Experiment on the PRISMA Mission; AIAA Guidance, Navigation, and Control Conference, 8-11 Aug. 2011, Portland, USA (2011). Journal of Guidance, Control and Dynamics (2012, in print).David A. Vallado, Fundamentals of Astrodynamics and Applications (2nd Edition).